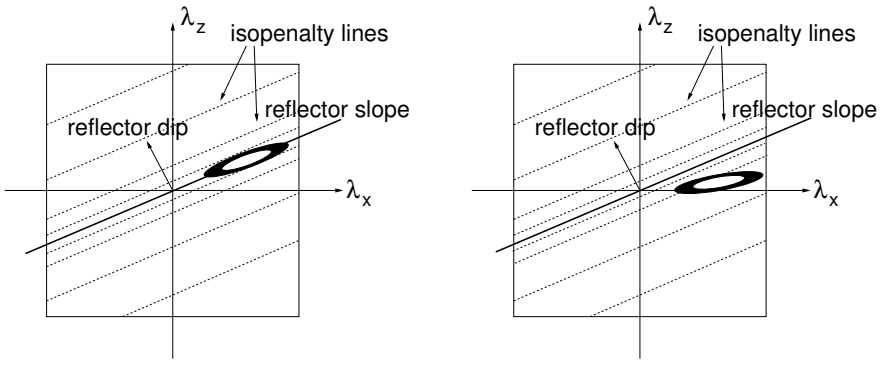

Figure 1: Cartoon describing the behavior of local correlation for the correct and for a incorrect model. The correlation of two images peaks in the direction aligned with the slope of the reflector (a); when the velocity is incorrect the correlation peaks away from it (b).

Introduction

Seismic imaging includes the estimation of both the *position* of the structures that generate the data recorded at the surface and a *model* that describes the propagation in the subsurface. The two problems are related since a model is necessary to infer the position of the reflectors. The waves recorded at the surface are extrapolated in the model by solving a wave equation, and they are crosscorrelated with a synthetic source wavefield simulated in the same model (Claerbout, 1985). Under a single scattering approximation, reflectors are located where the source and receiver wavefields match in time and space. If the velocity model is inaccurate, the reflectors are positioned at incorrect locations.

Wave-equation tomography is a family of techniques that estimate the velocity model parameters from finite bandwidth signals recorded at the surface. The inversion is usually formulated as an optimization problem, where the correct velocity minimizes a certain objective function that measures the inconsistency between the data simulated in a trial velocity model and the observed data. The objective function can be defined either in the data space (full-waveform inversion (Tarantola, 1984; Pratt, 1999; Sirgue and Pratt, 2004)) or in the image space (migration velocity analysis).

Migration velocity analysis (Fowler, 1985; Faye and Jeannot, 1986; Al-Yahya, 1989; Chavent and Jacewitz, 1995; Biondi and Sava, 1999; Albertin et al., 2006; Yang and Sava, 2010) defines the objective function in the image space and is based on the semblance principle (Al-Yahya, 1989). Groups of experiments and the associated images are analyzed. If the velocity model is correct, the images from different experiments must be consistent since a single earth model generates the recorded data. Migration velocity analysis leads to smooth objective functions and well-behaved optimization problems (Symes, 1991; Symes and Carazzone, 1991), and it is less sensitive to the initial model than full-waveform inversion. Migration velocity analysis measures either the invariance of the migrated images in an auxiliary dimension (reflection angle, shot, etc.) (Al-Yahya, 1989; Rickett and Sava, 2002; Xie and Yang, 2008) or focusing in an extended space (Rickett and Sava, 2002; Symes, 2008; Sava and Vasconcelos, 2009).

We propose a new objective function that operates in the image space and does not need common-image gathers (CIGs). We consider pairs of images from adjacent experiments and reformulate the semblance principle in the physical space, instead of the extended space at selected CIGs. We use the local correlations of two images to define an objective function based on multi-dimensional shifts in the image space. This approach allows us to include all image points in the velocity analysis step.

Theory

Migration velocity analysis is based on the semblance principle (Al-Yahya, 1989): a single earth model generates the recorded data and if the velocity model is correct, different experiments must produce consistent images of the reflectors.

Two possible measures of similarity between two images are their difference and their correlation.

We evaluate the semblance of two images by computing local correlations at each image point and define the objective function

$$\mathcal{J}(m) = \frac{1}{2}\sum_i \| K(\mathbf{x}) \sum_{\boldsymbol{\lambda}} P(\mathbf{x},\boldsymbol{\lambda})\, c_i(\mathbf{x},\boldsymbol{\lambda}) \|^2_{\mathbf{x}}, \tag{1}$$

where $c_i(\mathbf{x},\boldsymbol{\lambda}) = \int_{w(\mathbf{x})} R_{i+1}\left(\boldsymbol{\xi} - \frac{\boldsymbol{\lambda}}{2}\right) R_i\left(\boldsymbol{\xi} + \frac{\boldsymbol{\lambda}}{2}\right) d\boldsymbol{\xi}$ is the local correlation of the iamges R_i and R_{i+1} corresponding to shots with index i and $i+1$, and P is a penalty operator that highlights features that are related to velocity errors. The correlations are computed over the windows $w(\mathbf{x})$. Local correlations measure phase shifts between two images, thus our approach is robust against amplitude mismatches between shots (unlike an objective function based on the difference of two images).

If the velocity model is correct, two images from neighboring experiments build up the final image along the direction of the reflectors. This is equivalent to having no moveout in shot-domain common-image gathers (Xie and Yang, 2008). The similarity between the two images is evaluated at every point through local correlations. If the velocity model is correct, the *maximum* of the correlation lies along the reflector slope (Figure 1(a)); otherwise the maximum of the correlation is displaced from the reflector slope in a direction that depends on the sign and extent of the velocity error (Figure 1(b)). A measure of velocity error is obtained by penalizing the local correlations perpendicular to the reflector slope (Figure 1). If the velocity model is correct, the penalty operator annihilates the signal in the local correlation panels, otherwise a residual is obtained and can be exploited for wavefield tomography.

We compute the gradient of the objective function with the adjoint-state method (Plessix, 2006). In equation 1, we have two images, R_i and R_{i+1}, and 4 wavefields $u = [u_{s,i}\ u_{r,i}\ u_{s,i+1}\ u_{r,i+1}]$, which are the state variables of the system. The main step of the adjoint-state method is the computation of the adjoint-state variables, which are the solution of the state-equation for a new source term g. The new adjoint sources are defined as the partial derivative of the objective function with respect to the state variables u. We consider the dip field a slowly varying function of state variables and neglect its derivative with respect to the state variables, although these can also be included in the adjoint-source calculation. The source-side adjoint source has the following expressions:

$$\begin{aligned} g_{s,\mathbf{x}_s}(\mathbf{x},\boldsymbol{\eta},t) &= \left[r_{\mathbf{x}_{s-1}}(\mathbf{x}) \int P(\mathbf{x},\boldsymbol{\lambda})\, w\left(\mathbf{x} - \boldsymbol{\eta} + \frac{\boldsymbol{\lambda}}{2}\right) R_{\mathbf{x}_{s-1}}(\boldsymbol{\eta} - \boldsymbol{\lambda})\ d\boldsymbol{\lambda} \right. \\ &+ \left. r_{\mathbf{x}_s}(\mathbf{x}) \int P(\mathbf{x},\boldsymbol{\lambda})\, w\left(\mathbf{x} - \boldsymbol{\eta} - \frac{\boldsymbol{\lambda}}{2}\right) R_{\mathbf{x}_{s+1}}(\boldsymbol{\eta} + \boldsymbol{\lambda})\ d\boldsymbol{\lambda} \right] u_{r,\mathbf{x}_s}(\boldsymbol{\eta},t)\,. \end{aligned} \tag{2}$$

Similarly, the receiver-side adjoint source is obtained by replacing the background receiver wavefield $u_{r,\mathbf{x}_s}$ with the background source wavefield $u_{s,\mathbf{x}_s}$ in equation 2. The gradient of the objective function is computed then as the zero-time, zero-space lag crosscorrelation in time (or frequency) of state and adjoint-state variables, analogously to the procedure employed in conventional FWI.

Synthetic Examples

For illustration, we consider the simple synthetic heterogeneous model shown in Figure 2(a). We generate full-acoustic data with absorbing bounday conditions. The optimal migrated image is shown in Figure 2(b). The initial model for migration is a severly smoothed version of the correct model and is shown in Figure 2(c). The initial image (Figure 2(d)) is misfocused, and the reflectors are shifted from their correct location. After 4 inversion steps we recover the model in Figure 2(e) and the associated migrated image in Figure 2(f); the reflectors are better focused and closer to the actual position of the interfaces in the correct model. The edges of the reflector are frowning because the sides of the model are not well illuminated and the gradient of the objective function does not affect them. Figure 3 shows the evolution of the objective function with the number of iterations. After 4 iterations the objective function converges and the image is not updated further.

Conclusions

We present a new approach to wavefield tomography based on a restatement of the semblance principle in the image space. We define an objective function using appropriately penalized local image correlations.

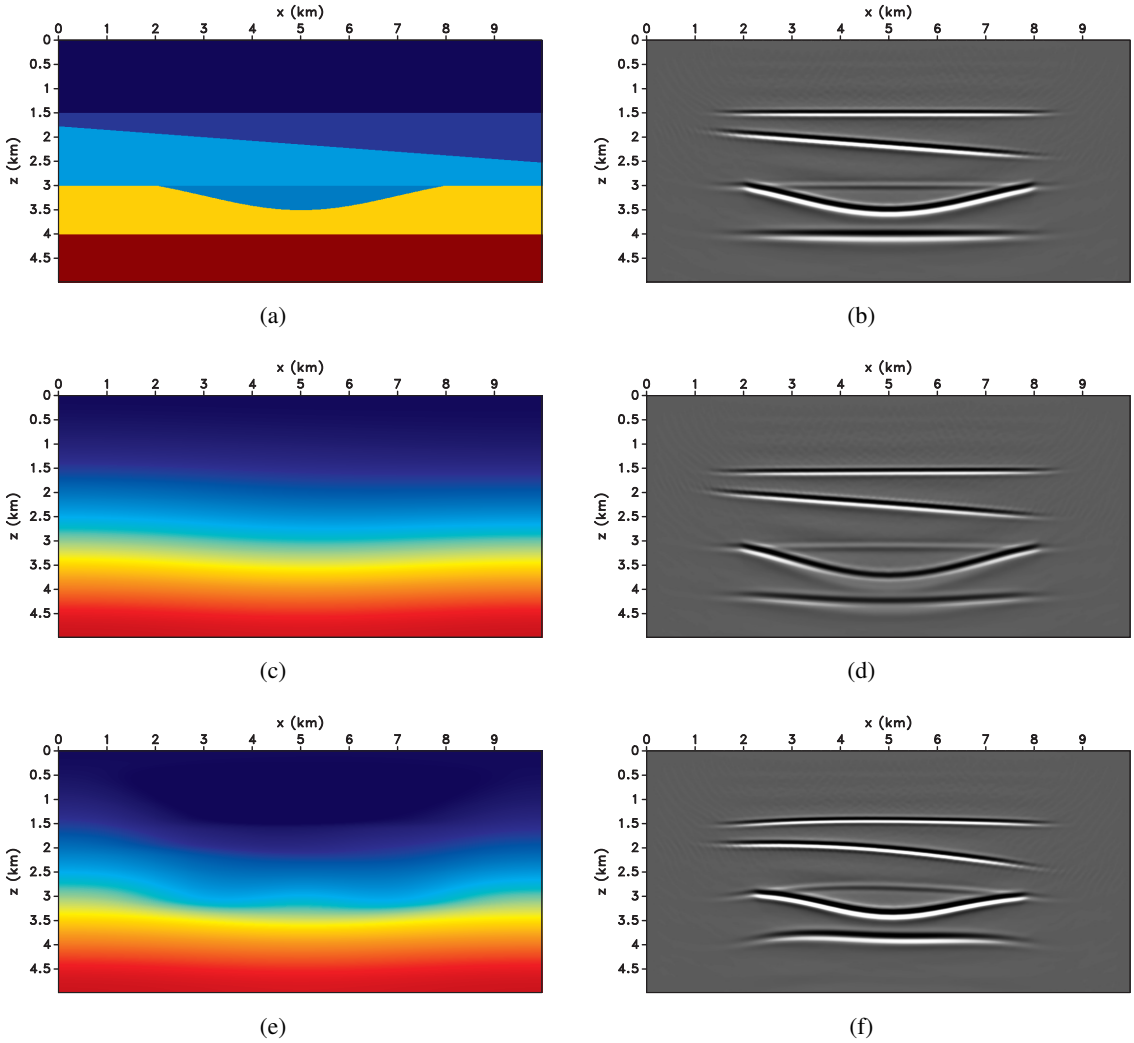

Figure 2: Velocity model used for generating the full-acoustic data (a) and the image obtained with the correct velocity model (b). The initial migration velocity model (b) and associated image (d). Migration velocity model after 4 inversion steps (e) and associated image (f). Observe the better focusing and positioning of the reflectors.

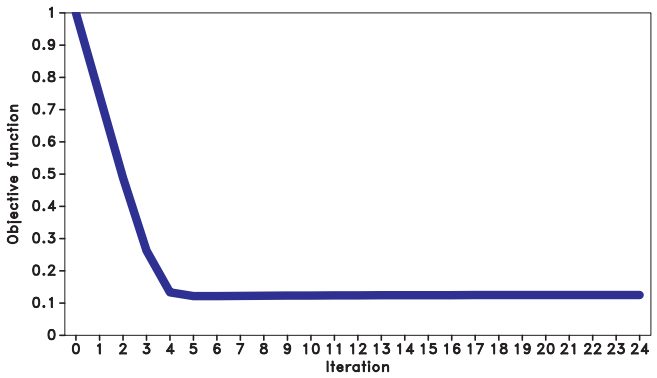

Figure 3: Evolution of the objective function with iterations. The inversion decreases the residual.

This formulation avoids both the construction of common-image gathers and the picking of moveout curves. The gradient with respect to the model parameters is computed with the adjoint-state method. A synthetic example with a laterally heterogeneous velocity model shows the ability of our strategy to measure the velocity error and focus the reflectors in the image space.

Acknowledgments

We would like to thank Eni E&P for the permission to publish this work. The reproducible numeric examples in this paper use the Madagascar open-source software package freely available from http://www.reproducibility.org.

REFERENCES

Al-Yahya, K., 1989, Velocity analysis by iterative profile migration: Geophysics, **54**, P. 718–729.

Albertin, U., P. C. Sava, J. Etgen, and M. Maharramov, 2006, Adjoint wave-equation velocity analysis: Presented at the 74th Ann. Internat. Mtg., SEG.

Biondi, B., and P. C. Sava, 1999, Wave-equation migration velocity analysis: Presented at the 69th Ann. Internat. Mtg., SEG.

Chavent, G., and C. A. Jacewitz, 1995, Determination of background velocities by multiple migration fitting: Geophysics, **60**, 476–490.

Claerbout, J. F., 1985, Imaging the earth's interior: Blackwell Publishing.

Faye, J.-P., and J.-P. Jeannot, 1986, Prestack migration velocity analysis from focusing depth imaging: Presented at the 56th Ann. Internat. Mtg., Soc. of Expl. Geophys.

Fowler, P., 1985, Migration velocity analysis by optimization: Technical Report 44, Stanford Exploration Project.

Plessix, R.-E., 2006, A review of the adjoint-state method for computing the gradient of a functional with geophysical applications: Geophys. J. Int., **167**, 495–503.

Pratt, R. G., 1999, Seismic waveform inversion in the frequency domain, part 1: Theory and verification in a physical scale model: Geophysics, **64**, 888–901.

Rickett, J., and P. Sava, 2002, Offset and angle-domain common image-point gathers for shot-profile migration: Geophysics, **67**, 883–889.

Sava, P. C., and I. Vasconcelos, 2009, Extended common-image-point gathers for wave-equation migration: Presented at the 71th Ann. Internat. Mtg., European Association of Geoscientists and Engineers.

Sirgue, L., and R. Pratt, 2004, Efficient waveform inversion and imaging: A strategy for selecting temporal frequencies: Geophysics, **69**, 231–248.

Symes, W. W., 1991, Layered velocity inversion: A model problem from reflection seismology problem from reflection seismology: SIAM J. on Math. Analysis, **22**, pp. 680–716.

———, 2008, Migration velocity analysis and waveform inversion: Geophysical Prospecting, **56**, 765–790.

Symes, W. W., and J. J. Carazzone, 1991, Velocity inversion by differential semblance optimization: Geophysics, **56**, 654–663.

Tarantola, A., 1984, Inversion of seismic reflection data in the acoustic approximation: Geophysics, **49**, 71–92.

Xie, X.-B., and H. Yang, 2008, The finite-frequency sensitivity kernel for migration residual moveout and its applications in migration velocity analysis: Geophysics, **73**, S241–S249.

Yang, T., and P. C. Sava, 2010, Wave-equation migration velocity analysis with extended common-image-point gathers: Presented at the 80th Ann. Internat. Mtg., Soc. of Expl. Geophys.